

# Quantum mechanical effects in internal photoemission THz detectors

M.B. Rinzan, S. Matsik, A.G.U. Perera \*

*Department of Physics and Astronomy, Georgia State University, Atlanta, GA 30303, United States*

Available online 20 November 2006

## Abstract

The variation in spectral shape around the threshold frequencies between model and experimental responsivity spectra in heterojunction interfacial workfunction internal photoemission (HEIWIP) infrared detectors was investigated. This is attributed to the loss of photoexcited carriers, within the escape cone, prior to photoemission. The energy dependent transmission of excited carriers is incorporated to the existing photoemission model to show that emission around the threshold frequency is reduced considerably by quantum mechanical reflection of photoexcited carriers as observed in experimental results. In the new model, the photoemission of carriers become bias dependent.

© 2006 Elsevier B.V. All rights reserved.

*PACS:* 85.60.Gz; 79.60.-i; 78.66.-w

## 1. Introduction

In order to extend the threshold wavelength of homojunction [1] and heterojunction internal photoemission detectors [2], besides exploring ways to design interfacial barriers for photoelectric conversion of Terahertz photons, the escape mechanism of carriers excited by these photons also needs to be studied and validated. Many internal photoemission based detector models use an escape cone mechanism to calculate photoemission efficiencies, and to define their threshold wavelength [3,4], where the detector responsivity goes to zero. According to this model, the response around the threshold wavelength should have a reasonable rise, at least for short wavelength detectors. Experimental results of internal photoemission detectors, however, do not show this expected behavior. Additionally, the experimental response around the threshold wavelength has been weaker than that predicted by the existing models. Therefore, this paper presents a modified photoemission model which takes the loss arising from quantum mechanical reflection of

photoexcited carriers into account. The material combination used in the detectors studied, GaAs/AlGaAs, allows us to assume isotropic condition for the effective mass of carriers, and the high doping density used in the emitters allows treating the free carrier population as an electron gas.

The experimental results for both short wavelength and long wavelength designs support the proposed photoemission model. The photoemission loss of excited carriers considerably reduces the response around the threshold wavelength for both short- and long-wavelength designs. Meanwhile, the dynamic resistance of long wavelength detectors ( $\lambda_0 \sim 80$  micron) is generally low ( $\sim$  from 500 to 1000  $\Omega$  even at liquid Helium temperature) due to their low interfacial workfunction ( $\sim 15$  meV), thereby leading to low photovoltage signals, especially, around the threshold wavelength. Therefore, although one expects to see the designed threshold, this is masked by noise, causing the practical threshold of the detector be determined by the noise floor of the measurement setup. In general, for heterojunction interfacial workfunction internal photoemission (HEIWIP) detectors, the threshold does not vary with the applied bias due to the absence of space charge [5]. However, some long wavelength HEIWIP designs have shown a variation with the applied field [6], due to the fact that both the signal and the measurement noise floor

\* Corresponding author. Present address: NDP Optronics LLC, 236 St. Martins Drive, Mableton, GA 30126, United States. Tel.: +1 404 651 2279; fax: +1 404 651 1427.

*E-mail address:* [uperera@gsu.edu](mailto:uperera@gsu.edu) (A.G.U. Perera).

increases with the bias. In long wavelength HEIWIP detectors, where one could notice the increase in threshold with the applied bias [6], the competition between the increasing detector signal and the increasing noise limits the observed threshold wavelength well within the designed value.

The paper also discusses the elongation of the designed threshold in a short wavelength p-type HEIWIP detector. The observed threshold change may be due to photoelectric conversion of carriers tunneling through the barrier. In addition to the photoexcited carriers distributed within the escape cone, the photoemission model should also include the contribution to emission probability from photoexcited carriers (with a nonzero velocity component towards the interfacial barrier as well) tunneling through the barrier. Including this, however, is tedious, and needs quantum mechanical treatment of the scattering events prior to photoemission. To be consistent with the above argument an elongation of the threshold wavelength for the long wavelength (THz) detectors is expected too. However, the aforementioned practical reasons limit such observations.

## 2. Internal photoemission: present versus modified

### 2.1. Present model

The responsivity of an IWIP (interfacial workfunction internal photoemission) detector depends on the internal photoemission quantum efficiency  $\eta_i$ . The ideal emission probability,  $\eta_{\text{Ideal}}$ , is described by an escape cone model, which is defined as the fraction of excited carriers that has sufficient kinetic energy, associated with the momentum component ( $p_0$ ) normal to the interface, for emission. This is given to the first order by the modified Fowler yield equation for the case  $E_F \gg hv$  and  $hv \gg \Delta$  as

$$\eta_{\text{Ideal}} = \frac{(hv - \Delta)^2}{8E_F hv}. \quad (1)$$

According to this model, hot carriers directed outside the escape cone, defined by  $p_0^2 = 2m^*(E_F + \Delta)$ , will emit only if they get redirected into the cone by scattering events or reflection by the emitter film walls. These scattering events and wall reflections were incorporated into Eq. (1) by Vickers [7] and Dalal [8], independently. The assumption made in their work, i.e., energy lost due to hot carrier and phonon collisions, was taken in to consideration by Mooney and Silverman in improving the model [9] later. In a previous study, the internal photoemission efficiency for SiGe/Si HIP detectors was obtained using different effective masses for the strained SiGe doped absorber/emitter layer and the Si-substrate [10,11]. For non parabolic bands the effective mass is a function of the carrier energy. All these papers have ignored the fraction of carriers that have states within escape cone, lost due to quantum mechanical reflection.

For an isotropic material, the energy shells of photoexcitation and photoemission are shown in Fig. 1(a). The

shaded innermost volume corresponds to the free carrier density and the volume enclosed by the  $t$  shells  $E = \max(E_F, hv)$  and  $E = (E_F + hv)$  corresponds to the excited carrier density. The photoemitted carrier density corresponds to the volume of the shaded spherical cap. The escape cone is defined by the half angle  $\theta$ , where  $\theta = \cos^{-1}(\frac{|k_{\text{perp}}|}{|k|})$ . Here,  $|k_{\text{perp}}|$  is fixed by the interfacial workfunction,  $|k_{\text{perp}}| = \frac{\sqrt{2m^*(E_F + \Delta)}}{\hbar}$ . The plane  $k_y = |k_{\text{perp}}|$  defines the threshold for photoemission. The photoemission probability of a p-type HEIWIP detector designed for  $\lambda_0 = 15 \mu\text{m}$  is shown in Fig. 1. According to the “escape cone” model, the increase in emission probability corresponding to near threshold photons is larger than observed in experiments.

The maximum emission efficiency is defined as the ratio of the number of hot carriers that can be potentially captured to number of photoexcited carriers. For both  $\Delta < E_F$  and  $\Delta > E_F$  cases, the ideal ( $\eta_{\text{Ideal}}$ ) and maximum

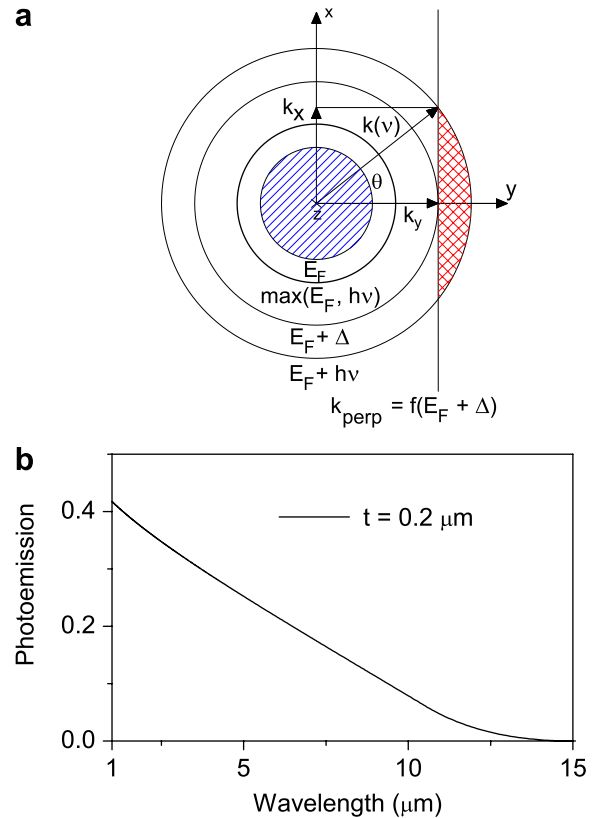


Fig. 1. (a) The diametral cross-section of the constant energy surface for a single valley of the emitter. The material is assumed to be isotropic for carrier transport, hence the density of state mass is similar to the effective mass. The shaded innermost volume corresponds to the free carrier density, the volume enclosed by the shells  $E = \max(E_F, hv)$  and  $E = (E_F + hv)$  corresponds to the excited carrier density, and the volume of the shaded spherical cap corresponds to the emitted carrier density. The escape cone is defined by the half angle  $\theta$ , where  $\theta = \cos^{-1}(\frac{|k_{\text{perp}}|}{|k|})$ . Here,  $|k_{\text{perp}}|$  is fixed by the interfacial workfunction,  $|k_{\text{perp}}| = \frac{\sqrt{2m^*(E_F + \Delta)}}{\hbar}$ . The plane  $k_y = |k_{\text{perp}}|$  defines the threshold for photoemission. (b) The photoemission probability of excited carriers with states in the spherical cap. This shows a rise around the threshold wavelength. The workfunction corresponds to  $15 \mu\text{m}$ .

( $\eta_M$ ) emission efficiencies of excited carriers are given by the following sets of equations.

For  $\Delta > E_F$ :

$$\eta_{\text{Ideal}} = 0 (E \leq \Delta), \quad (2)$$

$$\eta_{\text{Ideal}} = \frac{3}{4} \cdot \frac{\frac{2}{3} \cdot [(E_F + E)^{1.5} - (E_F + \Delta)^{1.5}] - (E - \Delta) \cdot (E_F + \Delta)^{0.5}}{(E_F + E)^{1.5} - E^{1.5}}, \quad (3)$$

$$\eta_M = \frac{1}{2} \cdot \frac{(E_F + E)^{1.5} - (E_F + \Delta)^{1.5}}{(E_F + E)^{1.5} - E^{1.5}} \quad (\Delta \leq E < E_F + \Delta),$$

$$\eta_{\text{Ideal}} = \frac{3}{4} \cdot \frac{\frac{2}{3} \cdot [(E_F + E)^{1.5} - (E)^{1.5}] - E_F \cdot (E_F + \Delta)^{0.5}}{(E_F + E)^{1.5} - E^{1.5}}, \quad (4)$$

$$\eta_M = \frac{1}{2} \quad (E_F + \Delta \leq E).$$

For  $\Delta < E_F$ , Eq. (3) breaks in to two different regions while others remain the same.

$$\eta_{\text{Ideal}} = \frac{3}{4} \cdot \frac{\frac{2}{3} \cdot [(E_F + E)^{1.5} - (E_F + \Delta)^{1.5}] - (E - \Delta) \cdot (E_F + \Delta)^{0.5}}{(E_F + E)^{1.5} - E_F^{1.5}}, \quad (5)$$

$$\eta_M = \frac{1}{2} \cdot \frac{(E_F + E)^{1.5} - (E_F + \Delta)^{1.5}}{(E_F + E)^{1.5} - E_F^{1.5}} \quad (\Delta \leq E < E_F),$$

$$\eta_{\text{Ideal}} = \frac{3}{4} \cdot \frac{\frac{2}{3} \cdot [(E_F + E)^{1.5} - (E_F + \Delta)^{1.5}] - (E - \Delta) \cdot (E_F + \Delta)^{0.5}}{(E_F + E)^{1.5} - E^{1.5}}, \quad (6)$$

$$\eta_M = \frac{1}{2} \cdot \frac{(E_F + E)^{1.5} - (E_F + \Delta)^{1.5}}{(E_F + E)^{1.5} - E^{1.5}} \quad (E_F \leq E < E_F + \Delta).$$

Here,  $E$  is the energy of the incident radiation,  $\Delta$  is the interfacial workfunction, and  $E_F$  is the Fermi energy of the emitter. The ideal efficiency is modified through scattering processes involving cold electrons (characterized by the scattering length,  $L_e$ ), elastic scattering with phonons and impurities (characterized by the scattering length,  $L_p$ ), and multiple reflections of the excited carriers from the surfaces of the emitter (from both the emitter/ambient-medium and emitter/barrier walls). These effects have been incorporated to the emission model in Refs. [7 and 9]. The fraction of hot carriers ( $\eta_0$ ) captured prior to any bulk scattering events, is well approximated by:

$$\eta_0 = \frac{L^*}{W} \cdot (1 - e^{-\frac{W}{L^*}})^{\frac{1}{2}} \cdot \eta_{\text{Ideal}}, \quad (7)$$

where  $(1 - e^{-\frac{W}{L^*}})^{\frac{1}{2}}$  is the probability of having no scattering from bulk collisions during multiple traversals within the

emitter (due to reflections of hot carriers from its walls), and  $L^* = \frac{L_e \cdot L_p}{L_e + L_p}$  is the reduced scattering length of a hot carrier.

The actual photoemission probability ( $\eta_i$ ) of a hot carrier, taking into account the scattering with cold carriers and phonons, is given by:

$$\eta_i = \eta_0 + \left[1 - \frac{\eta_0}{\eta_M}\right] \gamma \eta_1 + \left[1 - \frac{\eta_0}{\eta_M}\right] \cdot \left[1 - \frac{\eta_1}{\eta_M}\right] \gamma^2 \eta_2 + \dots,$$

where  $\eta_n \equiv \eta_0(E - nh\nu)$  and  $\gamma = \frac{L_e}{L_e + L_p}$  is the probability that the hot carrier will collide with a phonon before it collides with a cold electron. Here,  $n$  is the number of scattering events after which the thermalization ceases for a given hot carrier.

## 2.2. Modified model

The proposed model is the convolution of the transmission probability of photoexcited carriers and the photoemission efficiency given by the “escape cone model”. For example, if there is no loss arising from reflection then the proposed model derives the same probability given by the escape cone model ( $\eta_i$ ). According to the proposed model, the photoemitted carrier density prior to bulk scattering event is given by:

$$N_{\text{Emitted}} = \int_{\max(E_F + \Delta, h\nu)}^{E_F + h\nu} g(E - h\nu) dE \times \int_0^{\theta_{\max}} \sin \theta \cdot T(E \cos^2 \theta) d\theta, \quad (8)$$

where  $g(E - h\nu)$  is the density of initial states,  $\theta_{\max} = \arccos\left(\frac{E_F + \Delta}{E_F + h\nu}\right)$  defines the escape cone of momentum for carriers with final energy  $E$ , and  $T(E \cos^2 \theta)$  is the transmission probability of the excited carriers with final energy  $E$  and incident angle  $\theta$ . The transmission  $T(E, \theta) = T(k_y, F)$  depends on the bias drop across a barrier unit as shown in Fig. 2 and given by [12]:

$$T(k_y, F) = \frac{4k_{\text{III}}}{\pi^2 k_1} \left( \left\{ [\text{Ai}(y_1) \text{Bi}'(y_{\text{III}}) - \text{Bi}(y_1) \text{Ai}'(y_{\text{III}})] + \frac{k_{\text{III}}}{k_1} [\text{Bi}'(y_1) \text{Ai}(y_{\text{III}}) - \text{Ai}'(y_1) \text{Bi}(y_{\text{III}})]^2 \right\} + \left\{ \frac{\lambda}{k_1} [\text{Ai}'(y_1) \text{Bi}'(y_{\text{III}}) - \text{Bi}'(y_1) \text{Ai}'(y_{\text{III}})] + \frac{k_{\text{III}}}{\lambda} [\text{Ai}(y_1) \text{Bi}(y_{\text{III}}) - \text{Bi}(y_1) \text{Ai}(y_{\text{III}})] \right\}^2 \right)^{-1} \quad (9)$$

where  $y_1 = \left(\frac{2m}{e^2 F^2 \hbar^2}\right)^{1/3} \cdot (\Delta E_C - E_y)$ ,  $y_{\text{III}} = \left(\frac{2mF}{e^2 F^2 \hbar^2}\right)^{1/3} \cdot (\Delta E_C - E_y - eFW_2)$ , and  $\lambda = -\left(\frac{2m e F}{\hbar}\right)^{1/3}$ . Here,  $m$  is the effective mass of the electrons,  $F$  is the field in the barrier,  $E_y$  is the  $y$ -component of energy of the electrons incident on the barrier,  $\text{Ai}$  and  $\text{Bi}$  are the Airy functions. Here,  $k_1 = \frac{\sqrt{2mE_y}}{\hbar}$  and  $k_{\text{III}} = \frac{\sqrt{2m(E_y + eFW_2)}}{\hbar}$ .

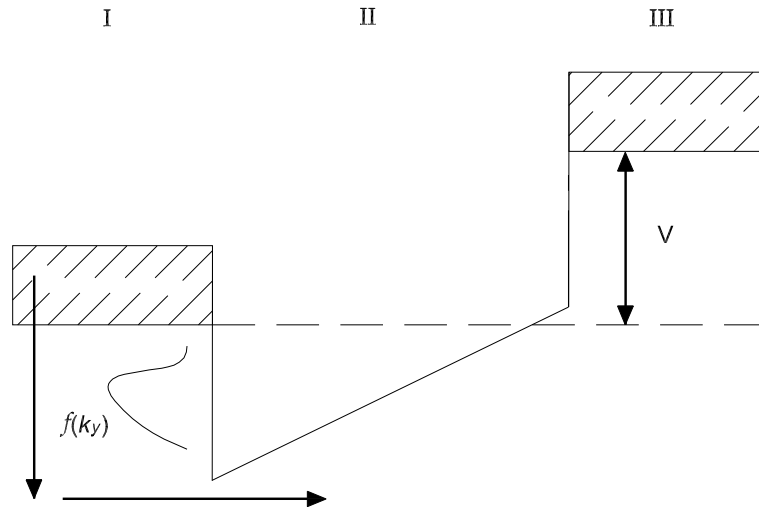


Fig. 2. A single barrier HEIWIIP detector under bias presenting a triangular (or trapezoidal) barrier for the photoexcited carriers. The three regions represent the wells and the barrier of the detector.

### 3. Experiment

The HEIWIIP detection mechanism involves infrared absorption by free carriers in the doped emitter layers followed by the internal photoemission of photoexcited carriers across the barrier interface and then collection [4]. A typical GaAs/AlGaAs HEIWIIP consists of a sequence of alternating GaAs emitters and AlGaAs barriers sandwiched between two highly doped contact layers. The spectral threshold,  $\lambda_0$  in micron, is given by  $1240/\Delta$ , where  $\Delta$  in meV is the interfacial workfunction. Here, results are reported on two detectors: One with GaAs emitters designed for short wavelength ( $\lambda_0 = 15 \mu\text{m}$ ), and the other with AlGaAs emitters designed for long wavelength ( $\lambda_0 = 174 \mu\text{m}$ ) operation. The main difference between the two is the inverted structure used in the long wavelength design, and the Al fraction of the AlGaAs layers. The absorption measurement carried out on doped  $\text{Al}_x\text{Ga}_{1-x}\text{As}$  epitaxial films with different Al composition,  $x$ , showed that the difference in the absorption coefficient is minimal. The structure parameters of the two detectors used in this study are given in Table 1. The HEIWIIP structures were grown by Molecular Beam Epitaxy (MBE) on semi-insulating GaAs (100) substrates. The samples were processed by delineating square mesa elements of four different areas from  $400 \times 400$  to  $1000 \times 1000 \mu\text{m}^2$  by wet

etching techniques. Ti/Pt/Au ohmic contacts were evaporated onto the top and bottom contact layers. Unlike in previous devices, the top contact was not etched for both detectors.

The transmission probability of the excited carriers for the detector designed for  $\lambda_0 = 174 \mu\text{m}$  (V0207) is shown in Fig. 3. The  $x$ -scale represents the final energy of the excited carriers and the vertical dashed line represents the energy corresponding to the top of the barrier. As seen in the figure, the reflection loss increases for carriers with energy closer to  $E_F + \Delta$ . In other words, the photoemission of carriers excited by photons close to the threshold suffers a significant loss due to reflection. In the previous model, the transmission was taken as unity for carriers excited by any photons below threshold. The loss becomes significant when the bias applied across the device is low. This means that in the presence of system noise, the signal around the threshold for a long wavelength detector would be buried within the noise, more so for low fields. This will result in recording a lower threshold than the detector was designed for, and also result in observing a threshold variation with the applied bias field.

This signature has been noticed in V0207 designed for operation up to  $175 \mu\text{m}$ . The maximum threshold of  $128 \mu\text{m}$  was obtained by taking the average of many spectra for a given field. It was noticed that when the bias

Table 1  
The structure parameters of detectors considered to demonstrate the effects of quantum mechanical reflection loss of photoexcited carriers

Detector	Top contact	Emitter layer		Barrier layer		Bottom contact	Periods	$\lambda_0$ ( $\mu\text{m}$ )
	Type	Type	$W$ ( $\mu\text{m}$ )	Type	$W$ ( $\mu\text{m}$ )			
1332	$\text{p}^+\text{-GaAs}$	$\text{p}^+\text{-GaAs}$	0.0188	$\text{Al}_{0.15}\text{Ga}_{0.85}\text{As}$	0.125	$\text{p}^+\text{-GaAs}$	12	15
V0207	$\text{p}^+\text{-Al}_{0.005}\text{Ga}_{0.995}\text{As}$	$\text{p}^+\text{-Al}_{0.005}\text{Ga}_{0.995}\text{As}$	0.05	GaAs	0.2	$\text{p}^+\text{-Al}_{0.005}\text{Ga}_{0.995}\text{As}$	10	174

The detector structures are grown on semi-insulating GaAs substrates. Notations  $W$ ,  $N$ , and  $\lambda_0$  denote the layer thickness, emitter/barrier periods, and the designed threshold wavelength of the detectors, respectively. The emitter doping density of detectors 1332 and V0207 are  $3 \times 10^{18}$  and  $5 \times 10^{18} \text{cm}^{-3}$ , respectively. Both detectors have a top contact thickness of  $0.2 \mu\text{m}$  and a bottom contact thickness of  $0.7 \mu\text{m}$ .

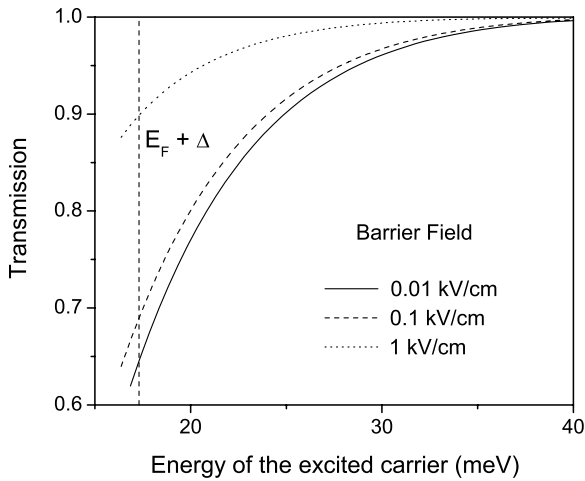


Fig. 3. Transmission probability for excited carriers as a function of their final energy. The energy is measured from the top of emitter valance band. The different curves show the variation of transmission with barrier field, which is determined by the bias applied across the device and the number of emitter/barrier units. The vertical dashed line shows the final energy corresponding to the threshold of the detector ( $\lambda_0 = 174 \mu\text{m}$ ).

across the detector was increased, it required more spectra in order to obtain a mean value for the threshold, which is a signature of the increasing noise. The shift in threshold for V0207 is shown in Fig. 4. Although other causes, such as band bending in the barrier, for this behavior are not yet ruled out, the combination of carriers generated by near threshold photons and the increasing system noise with the bias remains plausible in explaining the variation. As described above, when the bias increases the loss around threshold decreases increasing the signal. Therefore, if the system noise is constant with the bias one would expect to see an increasing threshold up to the design value. How-

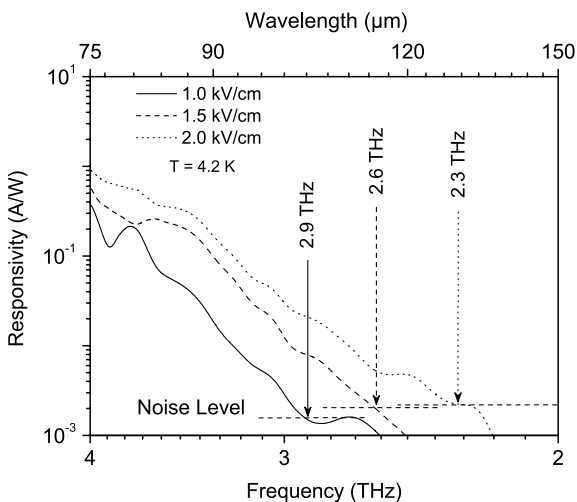


Fig. 4. Semi-log plot of the responsivity spectra, around the threshold wavelength, for detector V0207. The threshold increases with the bias to a maximum of  $128 \mu\text{m}$ . Any additional increase in the bias increases the noise floor disabling to obtain a threshold. The horizontal line segments intercepting the spectra are shown to indicate the noise levels for different biases. The full spectra can be found elsewhere [6].

ever, since the noise also increases with the bias the noise determined threshold cannot increase indefinitely and has a limit as shown in Fig. 4.

For the short wavelength designs, the effect of reflection is greater than it is for a long wavelength design. Fig. 5 demonstrates the large loss of excited carriers within the escape cone due to quantum mechanical reflections. However typical high dynamic resistance available in these detectors produces a very good response signal, and the threshold is not expected to be less than that of design. Detector 1332 designed for  $\lambda_0 = 15 \mu\text{m}$  operates up to  $16.7 \mu\text{m}$ . A possible reason for the observed extension is given in the conclusion. the spectral response of 1332 along with the response models, generated using the existing photoemission model and the proposed model, are shown in Fig. 6(a). The spectral shape below  $\sim 5 \mu\text{m}$  shoots up due to photoexcitation of carriers in the light and heavy hole bands to the split off band of the emitter layers. For GaAs, this transition is around  $3.5 \mu\text{m}$ . The proposed model gives a better fit around the threshold wavelength, as shown in Fig. 6(b), which was evaluated to be  $15 \mu\text{m}$  using SIMS data. In contrary to V0207, the experimentally determined threshold is slightly greater than the expected value. This may be due to the non-zero photoemission probability of photoexcited carriers with final energy slightly below the interfacial barrier. This is illustrated in Fig. 8.

Fig. 8 shows an excited carrier with its momentum directing outside the escape cone defined by the incident photon energy. Although it fails to emit ballistically, according to quantum mechanics, there is a non-zero probability of emission as the carrier is directed towards the barrier. This is valid for excited carriers with final energy slightly lower than the interfacial workfunction. Therefore,

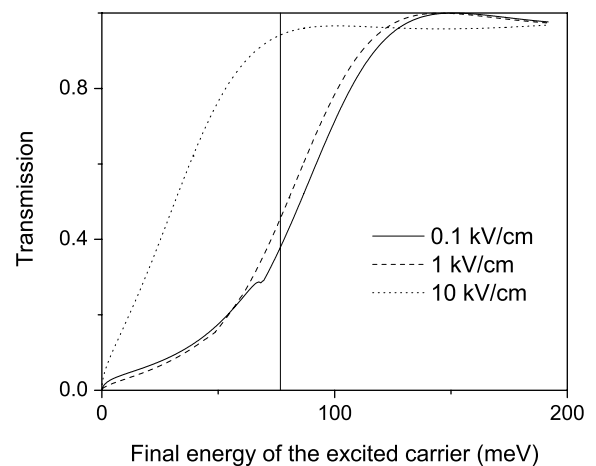


Fig. 5. Transmission probability of excited carriers for a detector designed for operation in the short wavelength regime. The x axis represents the final energy of excited carriers measured from the top of emitter valance band. The different curves show the variation with transmission with barrier field. Unlike for the long wavelength design, the reflection loss is significant at typical bias fields of  $\sim 1 \text{ kV/cm}$ . The minima in the transmission curves is generated by the interference of carriers traversing the barrier.

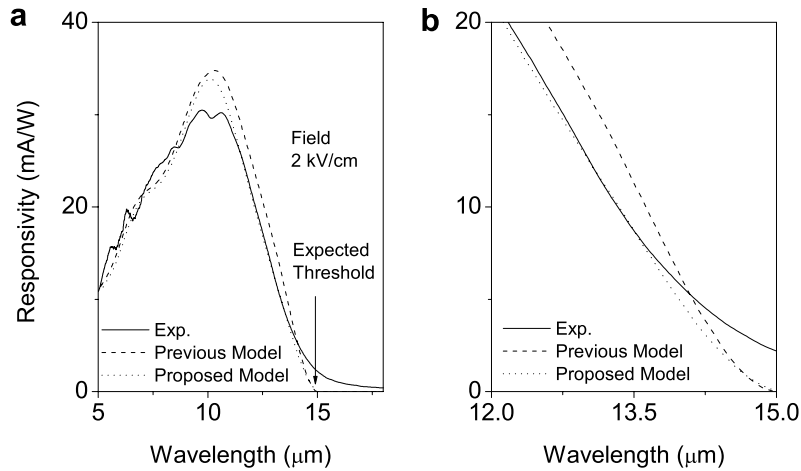


Fig. 6. (a) Experimental and model spectra for detector 1332. The threshold expected from SIMS parameters was 15  $\mu\text{m}$ , which is slightly less than the observed value. The elongation of expected threshold may be due to tunneling of photoexcited carriers near the barrier edge. (b) The zoomed in section around the threshold showing that proposed model agrees well with the experimental spectra around the threshold wavelength.

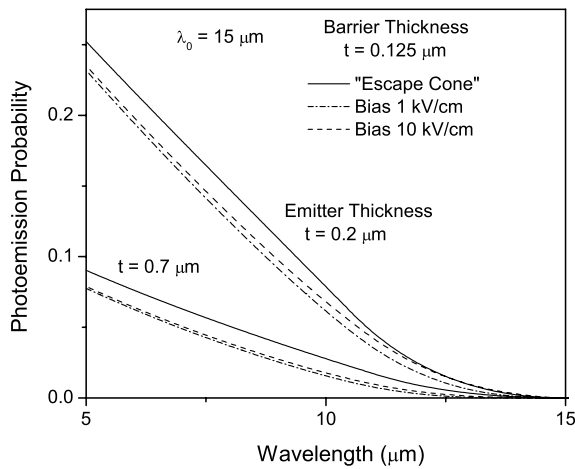


Fig. 7. Variation of photoemission probability with wavelength for a short wavelength design ( $\lambda_0 = 15 \mu\text{m}$ ). Unlike in the previous model, here, the photoemission efficiency is a function of the applied bias across the detector. This bias dependency is incorporated in to the model through the transmission probability of carriers, which is bias dependent. The emission increases with the applied bias. The solid line shows the emission evaluated from the “escape cone” model. The two groups are for different emitter thicknesses, with the emission decreasing with thickness.

an elongation of the ballistically defined threshold wavelength can be expected in HEIWIP detectors. The escape mechanism of carriers whose energy is less than the work-function has not been added in the model. An effort was made along this direction, and it was found that the scattering mechanisms prior to emission have to be treated in a “quantum mechanical” perspective, which is beyond the scope of this paper.

Bias dependence of emission probability has been studied elsewhere by adjusting the scattering length parameters [13]. However, there is no clear correlation between the scattering lengths or the bias field obtained so far. In the present model, since the transmission is incorporated into the “escape cone” model the photoemission probability

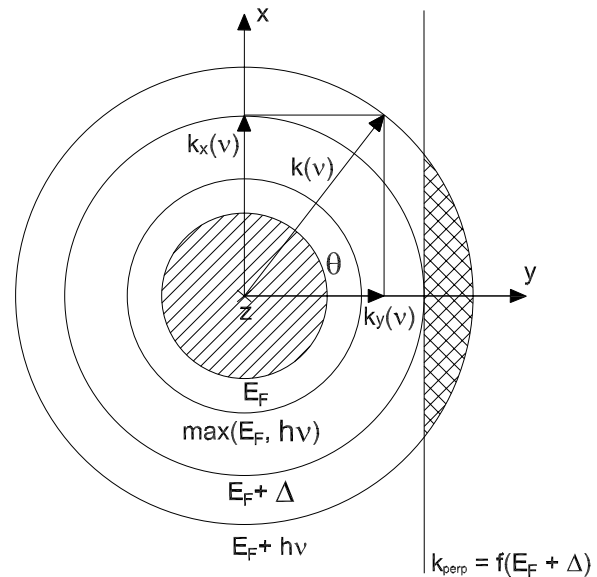


Fig. 8. Momentum space showing the escape probability of carriers even with less energy. The threshold is not well defined, and the experimental observation of the threshold wavelength is based on the system noise floor of the measurement.

now becomes a function of the applied bias or the bias field in the barrier. Fig. 7 shows the weak bias dependence of the photoemission probability. There is a small variation as the bias is increased by an order of magnitude, from 0.1 to 1 kV/cm. The figure also shows the photoemission curve corresponding to the “escape cone model”, and as predicted this is larger than the values derived from the proposed model.

#### 4. Conclusion

The effect of quantum mechanical reflection on the spectral response around the threshold of the detector has been discussed. The proposed photoemission model agrees with

the experimental results of short wavelength detectors and explains the threshold limitation seen in long wavelength designs. The tailing effect on the short wavelength detectors may be modeled by treating the scattering events quantum mechanically. Unlike in the escape cone model, the present model includes the dependence of photoemitted carrier density on the applied bias field.

### Acknowledgement

The work was supported in part by the US NSF under Grant No. ECS-0553051.

### References

- [1] A.G.U. Perera, W.Z. Shen, H.C. Liu, M. Buchanan, W.J. Schaff, GaAs homojunction interfacial workfunction internal photoemission (HIWIP) far-infrared detectors, *Mat. Sci. Eng. B* 74 (2000) 56.
- [2] D.G. Esaev, M.B.M. Rinzan, S.G. Matsik, A.G.U. Perera, Design and optimization of GaAs/AlGaAs heterojunction infrared detectors, *J. Appl. Phys.* 96 (2004) 4588.
- [3] H.C. Liu, L. Li, J.M. Baribeau, M. Buchanan, J.G. Simmons, Long wavelength infrared photocurrent study of Si–SiGe heterostructures, *J. Appl. Phys.* 71 (1992) 2039.
- [4] A.G.U. Perera, S.G. Matsik, B. Yaldiz, H.C. Liu, A. Shen, M. Gao, Z.R. Wasilewski, M. Buchanan, Heterojunction wavelength tailorable far infrared photodetectors with response out to 70  $\mu\text{m}$ , *Appl. Phys. Lett* 78 (2001) 2241.
- [5] H.X. Yuan, A.G.U. Perera, Space charge analysis of Si  $n^+ - i$  structures with application to far-infrared detectors, *Solid-State Electron.* 39 (1996) 621.
- [6] M.B.M. Rinzan, A.G.U. Perera, S.G. Matsik, H.C. Liu, Z.R. Wasilewski, M. Buchanan, AlGaAs emitter/GaAs barrier terahertz detector with a 2.3 THz threshold, *Appl. Phys. Lett.* 86 (2005) 071112.
- [7] V.E. Vickers, Model of Schottky barrier hot-electron-mode Photo-detection, *Appl. Opt.* 10 (1971) 2190.
- [8] V.L. Dalal, Simple model for internal photoemission, *J. Appl. Phys.* 42 (1971) 2274.
- [9] J.M. Mooney, J. Silverman, The theory of hot-electron photoemission in Schottky-barrier IR detectors, *IEEE Trans. Electron. Dev.* 32 (1985) 33.
- [10] B. Aslan, R. Turan, H.C. Liu, Study on the long wavelength SiGe/Si heterojunction internal photoemission infrared photodetectors, *Infrared Phys. Technol.* 195 (2005) 47.
- [11] B. Aslan, R. Turan, On the theory of internal photoemission in heterojunctions, *Infrared Phys. Technol.* 46 (2005) 473.
- [12] K.H. Gundlach, . . . resonant Fowler–Nordheim tunneling, *Solid-State Electron.* 9 (1966) 949.
- [13] A.G.U. Perera, H.X. Yuan, M.H. Francombe, Homojunction internal photoemission far-infrared detectors: Photoresponse performance analysis, *J. Appl. Phys.* 77 (1995) 915.